Nitrogen fixation by an arc plasma at elevated pressure to increase the energy efficiency and production rate of NO_x: Mechanistic insights from an equilibrium model

C. O'Modhrain, I. Tsonev, A. Bogaerts, Y. Gorbanev

Research group PLASMANT, Department of Chemistry, University of Antwerp, Belgium

Abstract: Plasma-based nitrogen fixation holds the potential to divert from primarily fossil-fuel based fertiliser production processes. However, the commonly observed inverse correlation between production rates and energy efficiency limits the current applicability. In this work, we highlight pressure as a key parameter for overcoming this barrier. Elevated pressures (up to ca. 4 atm) are experimentally shown to improve the production rate and product ratio of nitrogen oxides (NO_x). Insights gained from an equilibrium model provide insight into the underlying phenomena ascribed to this improvement.

Keywords: Nitrogen fixation, warm plasma, pressure, equilibrium model.

1. Introduction

Nitrogen fixation from large-scale, fossil-fuel based industrial processes is becoming less feasible and more costly (both financially and environmentally) in the current global climate. Most of the fertilisers in use are produced *via* the Haber-Bosch (HB) process. This energy intensive process uses 1-2 % of global energy annually, producing over 300 Mt of CO_2 per annum (not accounting for additional transport emissions) [1]. Plasma-based nitrogen fixation is a promising alternative, as the "turn-key" nature of the process combines more optimally with intermittent renewable energy resources than the HB process [2]. In addition, production units can be small-scale and decentralised, reducing reliance on fertiliser transportation.

The major drawback of such technologies to date is the commonly observed inverse correlation between the production rate and energy efficiency of the process. An overview of the current state-of-the-art for plasma-based nitrogen fixation is shown in Table 1.

Table 1. Overview of state-of-the-art plasma-based nitrogen fixation technologies

Entry	Discharge	N_2:O_2	Energy cost (MJ/(mol N))	Total NO_x production rate (g/h)	Ref
1	Pulsed AC spark	4:1	0.4	0.3	[3]
2	Pulsed DC spark	4:1	0.4	<0.1	[4]
3	DC glow	4:1	2.8	1.9	[5]
4	Microwave (surface wave)	1:1	2.0	85.9	[6]
5	Pulsed gliding arc	1:1	2.7	<0.1	[7]
6	Rotating gliding arc	1:1	1.8	68.9	[8]

Evidently, the systems with the lowest energy cost (*i.e.* Entries 1 & 2) are accompanied by very low nitrogen oxide (NO_x) production rates. While the energy cost (EC) associated with the warm plasma discharges (Entries 3-6) are slightly higher, the NO_x production rates (PRs) also increase, making these systems more industrially interesting and viable.

While experimental and theoretical research into high-pressure discharges has been thoroughly conducted [9],[10],[11], applications towards gas conversion are scarce in literature [12],[13],[14]. While high pressures, such as those used during the HB process (>250 atm), require specialised equipment, a slight plasma reactor environment overpressure (ca. 1-4 atm) is achievable with a needle valve and standard mass flow controllors (MFCs).

In this work, the effect of elevated pressure (ca. 1-4 atm) on the production rate and energy cost for nitrogen fixation using a rotating gliding arc (RGA) plasma reactor was initially experimentally investigated [8]. Following this, a fully-coupled, quasineutral equilibrium model was developed to gain insights into the reactor environment (*i.e.* flow and temperature fields, arc characteristics) and the dominant chemical pathways at play.

2. Experimental

The RGA plasma reactor used in this work is described in detail in our previous works applied to nitrogen fixation [15],[16]. The feed gases (N_2 and O_2) were supplied using MFCs and mixed using a T-connector, prior to being tangentially injected into the reactor (N_2:O_2 of 4:1 or 1:1, total flow rate of 4, 8 or 12 Ln/min) (Fig. 1). The reactor environment pressure was monitored using a manometer and controlled using a needle valve at the reactor outlet. The pressures investigated were 0-3 bar gauge pressure (barg) (ca. 1-4 atm).

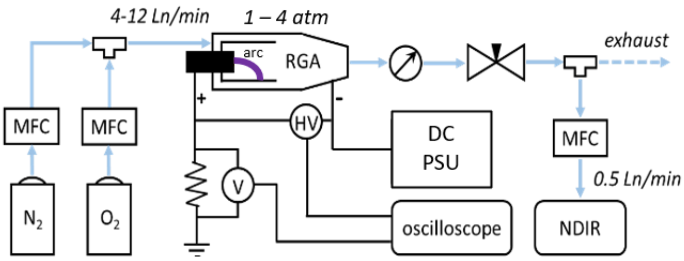

Fig. 1. Schematic representation of the RGA plasma reactor setup

The discharge was driven by a high-voltage, current-controlled DC power supply unit (PSU) (supplied current of 400 to 1000 mA) (Technix SR12KV-10KW). The electrical charcateristics were measured using a high-voltage probe (Tektronix P6015A) and a shunt resistor (2 Ω) connected to an oscilloscope (Keysight InfiniiVision DSOX1102A).

The effluent mixture was analysed in-line using a non-dispersive infrared (NDIR) sensor (Emerson, Rosemount X-stream Enhanced XEGP Continuous Gas Analyzer). In all experiments, the main products detected were NO and NO_2, the sum of which is the total NO_x concentration.

3. Modelling

A quasineutral equilibrium air model was developed in COMSOL Multiphysics (v.6.0) and solved using the finite element method. The model assumes the medium to be continuous, quasineutral, perfectly mixed and in a state of local thermodynamic equilibrium (LTE).

Thermodynamic and transport properties dependent on both pressure and temperature within a relevant range were applied using data retrieved from D'Angola [17]. The system of equations solved in a full-coupled manner include the conservation of mass, momentum, energy and current (Eqns. 1-4).

$$\frac{\partial \rho}{\partial t} + \nabla \cdot (u\rho) = 0 \tag{1}$$

$$\rho\frac{\partial u}{\partial t} + \rho(u \cdot \nabla)u = \nabla \cdot \left[-pI + \mu\left(\nabla u + (\nabla u^T)\right) - {}^{2}\!/_{3}\,\mu(\nabla \cdot u)I\right] \tag{2}$$

$$\rho C_p u \nabla T + \nabla \cdot (-k\nabla T) = Q_h \tag{3}$$

$$\nabla \cdot (\sigma E) = Q_e \tag{4}$$

Where ρ is the gas density (kg/m^3), u is the gas velocity (m/s), p is the gas pressure (Pa), I is the identity tensor, μ is the dynamic viscosity (Pa·s), T is the gas temperature, C_p is the heat capacity (J/kg.K), k is the thermal conductivity (W/m.K), Q_h is the heat source (W/m^3), σ is the electrical conductivity (S/m), E is the electric field (V/m) and Q_e is the electromagnetic heating term (W/m^3).

The results obtained from these simulations were used as input into a simple system of chemical reactions to elucidate the dominant pathways involved in the formation of NO_x. The species considered in this step were N_2, O_2, N, O, NO and NO_2.

A schematic drawing of the computational domain can be seen in Figure 2. A 2D-axisymmetric domain was opted for to decrease the computational cost. The axis of symmetry is denoted by the dashed line, and located at r = 0 mm (boundary AK).

To accurately capture the flow field, a 3D fluid flow model was initially solved and the resulting cylindrical vectors (u_r, u_θ, u_z) were extracted and set as initial inlet boundary conditions (boundary EF) in the 2D-axisymmetric domain.

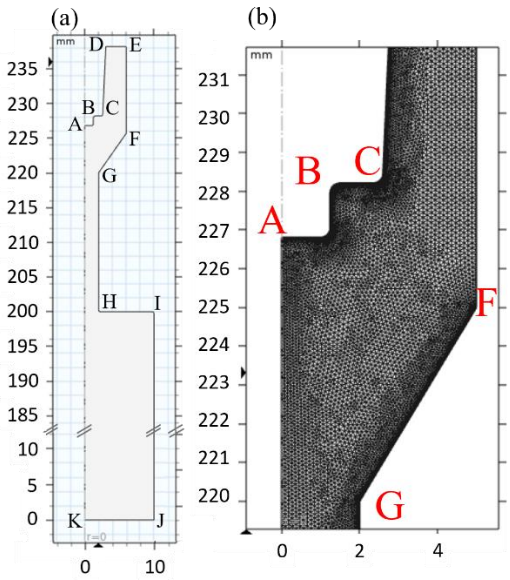

Fig. 2. 2D-axisymmetric computational domain (a) and close-up of the domain discretization (b)

Heat loss via natural convection was simulated on the reactor body (boundary FGHIK). As in the experiments, a DC current was supplied through the pin electrode (boundary AB), while the reactor body was grounded (boundary FGHIK).

4. Experimental results

4.1 Production of NO_x from air (N_2:O_2 ratio of 4:1)

The effect of elevated pressure on the production rate (PR) and energy cost (EC) of NO_x production was examined at first using an N_2:O_2 ratio of 4:1, mimicking dry air. For simplicity and consistency, the results are plotted as a function of the PSU supplied current. This PSU current varied from the measured plasma-deposited current, the latter of which was used in the power and EC calculations. In addition, only supplied currents that enabled a stable discharge (takeover mode) were used.

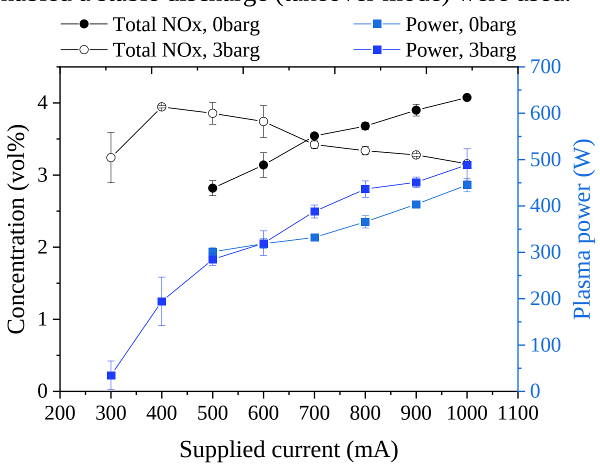

Fig. 3. Total concentration of produced NO_x and plasma power with N_2:O_2 ratio of 4:1, as a function of the PSU current at 4Ln/min for 0 barg (whole) and 3 barg (hollow)

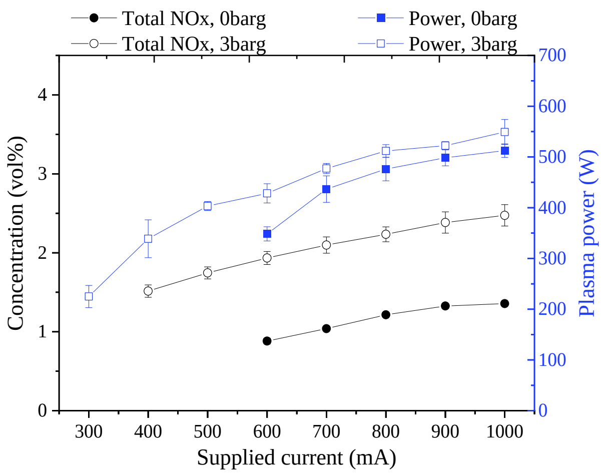

Fig. 4. Total concentration of produced NO_x and plasma power with N_2:O_2 ratio of 4:1, as a function of the PSU current at 12 Ln/min for 0 barg (whole) and 3 barg (hollow)

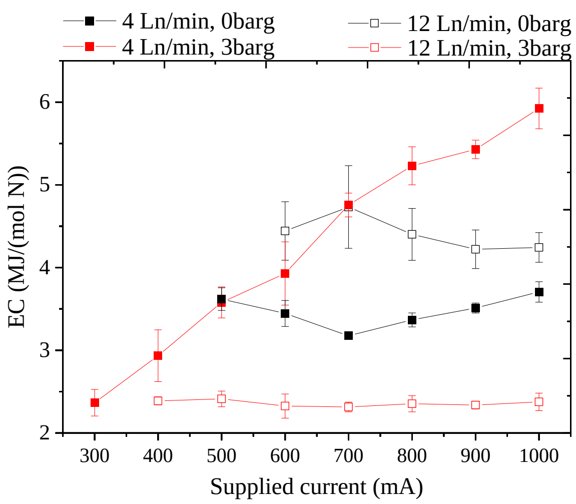

Fig. 5. Energy cost (EC) of NO_x production with N_2:O_2 ratio of 4:1, as a function of the PSU current at 4 and 12 Ln/min, and 0 barg (black) and 3 barg (red)

For 4 Ln/min at 0 barg, both the NO_x concentration and power increased as a function of the supplied current. As these factors increased proportionally to one another, the EC remained relatively constant (ca. 3.5 MJ/(mol N)). Upon increasing the pressure to 3 barg, the concentration of NO_x initially increased, peaked and then decreased as a function of increasing supplied current.

For 12 Ln/min at 0 barg, both the NO_x concentration and power increased as a function of the supplied current. Similar to the lower flow case, these factors increased relatively proportionally, leading to a reasonably constant EC (ca. 4.2 MJ/(mol N) for this condition (albeit at a higher value compared to the 4 Ln/min case). The benefit of higher flow rates becomes evident at elevated pressure, as for 12 Ln/min and 3 barg, the NO_x concentration constantly increased as a function of supplied current. As the amount of NO_x produced increased more significantly than the power required to sustain the discharge, an EC as low as 2.4 MJ/(mol N) was achieved.

4.2 Production of NO_x from oxygen-enriched air (N_2:O_2 ratio of 1:1)

As highlighted in Table 1, the most promising results for plasma-based nitrogen fixation are often obtained with an oxygen-enriched mixture. The increased presence of oxygen is advantageous for the formation of NO_x, but the discharges produced are often less stable, requiring more power to sustain a discharge at a constant current (compared to N_2:O_2 ratio of 4:1). Such enriched mixtures are obtainable through practices such as pressure swing absorption.

Figure 6 shows the EC and PR values obtained for flow rates of 4 and 12 Ln/min, at the highest pressure investigated (3 barg).

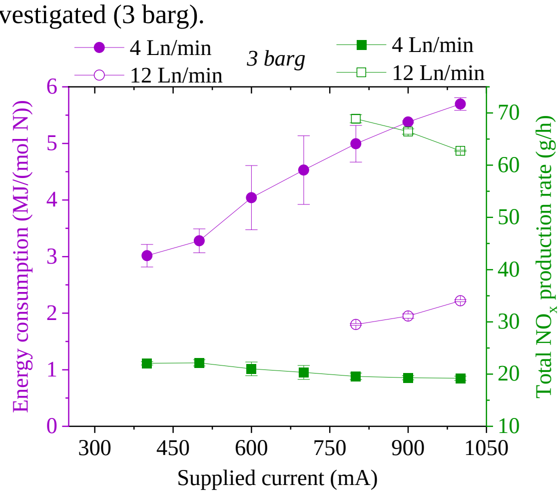

Fig. 6. Energy cost (EC) and total NO_x production rate (PR) with N_2:O_2 ratio of 1:1, as a function of the PSU current, for 4 and 12 Ln/min at an elevated pressure of 3 barg

Similar to the trend observed for 4 Ln/min with N_2:O_2 ratio at 4:1 and a pressure of 3 barg, the NO_x peaks at low supplied current values and declines for values above 400 mA. This poor conversion trend resulted in the EC increasing steadily as function of the supplied current. This trend was accompanied by a slight decrease in PR (ca. 20 g/h).

For 12 Ln/min, with N_2:O_2 ratio of 1:1 and at a pressure of 3 barg, a stable discharge could only be produced at supplied currents of 800 mA and above. Nonetheless, the lowest EC value for plasma-based NO_x production with a correspondingly high production rate (> 10 g/h) was recorded under these conditions, *i.e.*; 1.8 MJ/(mol N).

5. Modelling results

In the absence of an arc, the tangential injection of pure, dry air (N_2:O_2 ratio of 4:1) into the computational domain results in a reverse vortex flow.

Once fully-coupled, that is to say that the Navier-Stokes, heat balance and current conservation equations (Eqns. 1-4) are solved simultaneously, the swirling flow serves to isolate the arc from the reactor wall. This is evident from the temperature distribution within the domain, as shown in Figure 7a. The high core temperature results in gas expansion and acceleration out of the narrow region, as seen in Figure 7b. This increased convective flux influences the chemistry within the reactor, as shown in Figure 8.

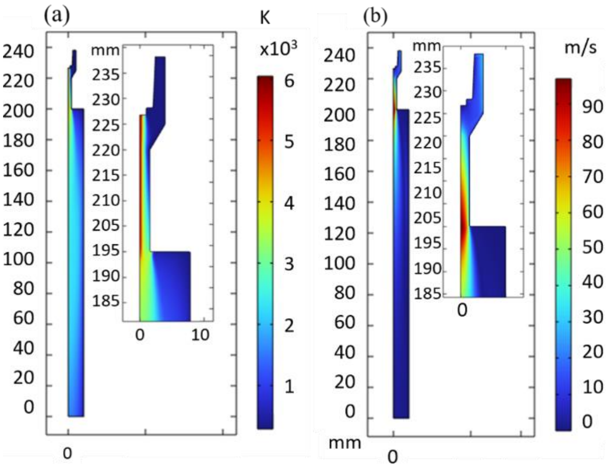

Fig. 7. Temperature (a) and velocity magnitude (b) distribution in the entire computational domain and reactor body (inset) 4 Ln/min, 0 barg and 500 mA.

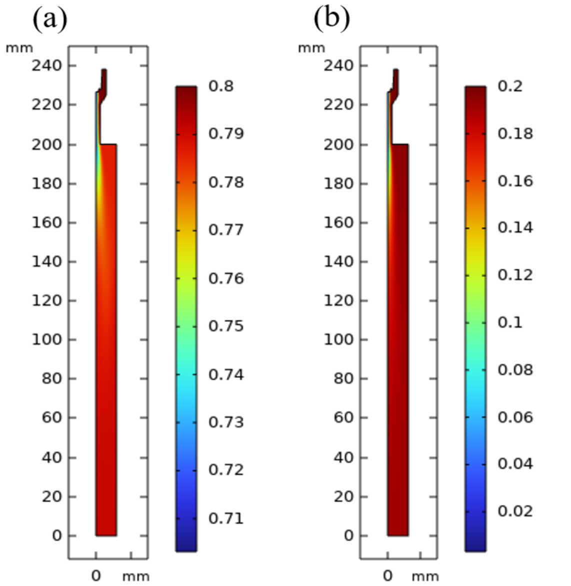

Fig. 8 Distribution plots of (a) mole fraction of N_2 and (b) mole fraction of O_2 in the entire computational domain for a supplied current of 500 mA, at 4 Ln/min and 0 barg.

The high temperature within the arc core (~ 6000 K) leads to complete dissociation of the molecular components of air. Figure 8a demonstrates this effect for N_2, dissociating into atomic N, whereas Figure 8b shows the same for O_2. Outside of the high-temperature core, the atomic species competitively recombine to form either N_2, O_2 or NO. Further oxidation of NO into NO_2 by atomic O originating from the high-temperature areas also occurs in the post-discharge region. As observed experimentally, the effect of increasing pressure results in an increased power deposition at a constant current value. This additional power potentially translates to arc elongation, increasing both the size of both the dissociation (arc core) and recombination (post-discharge) zones, allowing for increased NO_x production at elevated pressure (for high flow conditions).

6. Conclusion

The effect of elevated pressure (0 – 3 barg) on the performance of a rotating gliding arc (RGA) reactor for plasma-based nitrogen fixation was investigated, both experimentally and through modelling. The experiments revealed that increasing the pressure in the plasma reactor lead to an increased production rate (PR) for NO_x, while simultaneously decreasing the energy cost (EC) of the process. Insights from an equilibrium model highlighted the importance of the post-discharge region characterstics, such as flow and temperature fields, on the final NO_x concentration (and thus PR and EC).

This work identifies pressure as an important parameter for the increased performance of plasma-based nitrogen fixation, while simultaneously delving into the underlying mechanisms occurring within the reactor environment.

7. References

[1] C. Smith *et al.*, *Energy & Environmental Science*, **13**, 331-344 (2020).
[2] L. R. Winter *et al.*, *Joule*, **5**, 300-315 (2021).
[3] E. Vervloessem *et al.*, *Green Chemistry*, **24**, 916-929 (2022).
[4] N. Britun *et al.*, *Plasma Sources Science and Technology*, **30**, 08LT02 (2021).
[5] X. Pei *et al.*, *Journal of Physics D: Applied Physics*, **53**, 044002 (2019).
[6] S. Kelly *et al.*, *Joule*, **5**, 3006-3030 (2021).
[7] B. S. Patil *et al.*, *Aiche Journal*, **64**, 526-537 (2018).
[8] I. Tsonev *et al.*, *ACS Sustainable Chemistry & Engineering*, **XX**, XXX (2023).
[9] M. S. Benilov, *Journal of Physics D: Applied Physics*, **41**, 144001 (2008).
[10] L. Fulcheri *et al.*, *Plasma Sources Science and Technology*, **19**, 045010 (2010).
[11] P. Gueye *et al.*, *Journal of Physics D: Applied Physics*, **52**, 145202 (2019).
[12] B. Eliasson *et al.*, *Industrial & Engineering Chemistry Research*, **37**, 3350-3357 (1998).
[13] Y. Uytdenhouwen *et al.*, *Chemical Engineering Journal*, **372**, 1253-1264 (2019).
[14] S. Iwarere *et al.*, *Chemical Engineering Journal*, **241**, 1-8 (2014).
[15] F. Jardali *et al.*, *Green Chemistry*, **23**, 1748-1757 (2021).
[16] S. Van Alphen *et al.*, *Chemical Engineering Journal*, **443**, 136529 (2022).
[17] A. D'Angola *et al.*, *The European Physical Journal D*, **46**, 129-150 (2007).